

From Chaos to Coherence: Effects of High-Order Synaptic Correlations on Neural Dynamics

Nimrod Sherf^{1,2,*}, Xaq Pitkow^{2,3,4,5,6,†}, Krešimir Josić^{1,7,‡} and Kevin E. Bassler^{1,8,9§}

¹*Department of Mathematics,
University of Houston, Houston, Texas,
USA,*

²*Department of Neuroscience,
Baylor College of Medicine, Houston,
Texas, USA,*

³*Neuroscience Institute,
Carnegie Mellon University,
Pittsburgh, Pennsylvania, USA,*

⁴*Department of Machine Learning in the School of Computer Science,
Carnegie Mellon University,
Pittsburgh, Pennsylvania, USA,*

⁵*Departments of Electrical and Computer Engineering,
and Computer Science,
Rice University, Houston, Texas, USA,*

⁶*NSF AI Institute for Artificial and Natural Intelligence,*

⁷*Department of Biology and Biochemistry,
University of Houston, Houston,
Texas, USA,*

⁸*Department of Physics,
University of Houston, Houston, Texas,
USA,* ⁹*Texas Center for Superconductivity,
University of Houston, Houston, Texas, USA.*

(Dated: April 2, 2025)

Recurrent Neural Network models have elucidated the interplay between structure and dynamics in biological neural networks, particularly the emergence of irregular and rhythmic activities in cortex. However, most studies have focused on networks with random or simple connectivity structures. Experimental observations find that high-order cortical connectivity patterns affect the temporal patterns of network activity, but a theory that relates such complex structure to network dynamics has yet to be developed. Here, we show that third- and higher-order cyclic correlations in synaptic connectivities greatly impact neuronal dynamics. Specifically, strong cyclic correlations in a network suppress chaotic dynamics, and promote oscillatory or fixed activity. The change in dynamics is related to the form of the unstable eigenvalues of the random connectivity matrix. A phase transition from chaotic to fixed or oscillatory activity coincides with the development of a cusp at the leading edge of the eigenvalue support. We also relate the dimensions of activity to the network structure.

A central goal of theoretical neuroscience is to relate the structure, dynamics, and function of biological neural networks [1–8]. Model networks with random, Erdős–Rényi connectivity have been studied extensively, and exhibit a range of explainable dynamical behaviors, from fixed points and periodic orbits to highly chaotic states [1]. However, biological neuronal networks have highly structured connectivity [9–16]. While much effort has been devoted to understanding how such structure impacts neural dynamics and function, most work has focused on the impact of pairwise correlations, or structures encompassing the entire network [13, 17–21].

Mounting evidence suggests that cortical architecture is characterized by high-order correlations between synaptic connections [9, 11, 15, 16, 22–24]. Motifs com-

posed of three or more neurons are over-represented, and shape neural activity [24–31], yet the impact of such structure on neural dynamics and function remains poorly understood. While progress has been hindered by limits on our understanding of networks with higher order correlations in connectivity, advances in random matrix theory [32–36], and statistical physics [19, 37, 38] are paving the way for new insights.

Here, using numerical simulations we show that third- and higher-order cyclic correlations in synaptic connectivities have a strong impact on neuronal dynamics. We then characterize the connectivity structure through eigenvalue spectra and relate it to the network dynamics, showing how the emergence of irregular activity is strongly affected by high-order correlations in connectivity. We find that strong, positive high-order correlations tend to stabilize neuronal dynamics and reduce the dimensionality of activity. In contrast, strong, negative high-order correlations lead to high-frequency rhythmic behavior. Our results suggest that networks with such connectivity structure do not display chaotic behavior,

* nsherf@uh.edu

† xaq@cmu.edu

‡ kresimir.josic@gmail.com

§ bassler@uh.edu

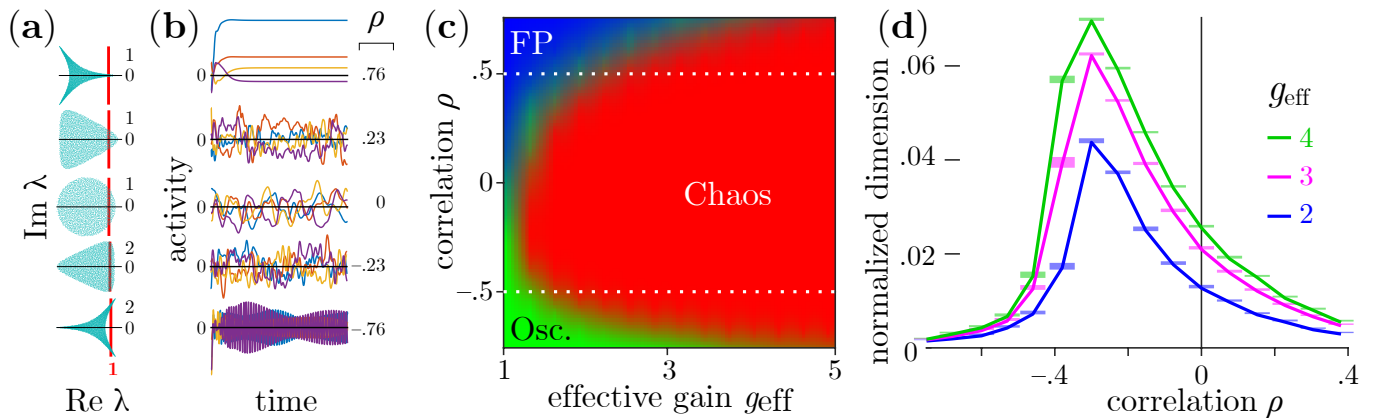


FIG. 1: Behavior of networks with third-order cyclic correlations: (a) Distributions of complex connectivity matrix eigenvalues λ at different correlation strengths ρ for effective gain $g_{\text{eff}} = 1.25$. The red lines correspond to $\text{Re } \lambda = 1$; eigenvalues to the right of the red line are unstable. (b) Activities of five typical neurons at each value of ρ . (c) Heat map showing probabilities of observing chaotic, oscillatory, or fixed point activity (red, green, and blue, correspondingly) as a function of g_{eff} and ρ . Dashed lines correspond to $\rho = \pm 0.5$. (d) Averaged normalized attractor dimension (participation ratio) at constant values of g_{eff} as a function of ρ .

unlike unstructured [1] and partially symmetric networks [21].

We consider a rate model of neuronal activity in a network of N neurons [1, 19, 20, 39],

$$\dot{x}_i(t) = -x_i(t) + \sum_{j=1}^N w_{ij} \phi(x_j(t)), \quad i = 1, \dots, N, \quad (1)$$

where x_i is the membrane potential of neuron i , $\phi(x_j) = \tanh(x_j)$ is the activation function of neuron j , and w_{ij} is the weight of the synaptic connection from neuron j to neuron i . Weights satisfy $\langle w_{ij} \rangle = 0$, $\langle w_{ij}^2 \rangle = \frac{g^2}{N}$, and

$$\underbrace{\langle w_{ij} w_{jk} w_{kl} \dots w_{pi} \rangle}_{\alpha} = \frac{g^\alpha \rho}{N^{\alpha-1}} \quad (2)$$

where the angular brackets $\langle \dots \rangle$ denote the ensemble average. The gain parameter g determines the coupling strength, ρ controls the strength of high-order directed cyclic correlations, and α denotes correlation order. We used a modification of the algorithm proposed by Aceituno, et al. [36] to generate matrices with the desired statistics (see section IA).

The eigenvalue spectrum of random matrices with high-order cyclic correlations obeys a Hypotrochoid Law [32, 33, 36]: The eigenvalue density when $\rho \ll 1$ and $N \rightarrow \infty$ has support inside the hypotrochoid $z(\phi) = g(e^{i\phi} + \rho e^{-i(\alpha-1)\phi})$. In contrast to uncorrelated or pairwise correlated weights, the eigenvalue density when $\alpha \geq 3$ is not uniform within the hypotrochoid, [36, 40–42]. At finite values of $|\rho|$ we observe deviations from the Hypotrochoid Law (See Fig. S2): At small values of $|\rho|$, eigenvalues can be found just outside the hypotrochoid, and at $|\rho| > \rho_c$, where $\rho_c \equiv (\alpha - 1)^{-1}$, hypotrochoids have loops, which the eigenvalue density does not follow.

The Hypotrochoid Law, nevertheless, provides an approximation of the real part of the leading (rightmost) eigenvalue, which we call the effective gain, g_{eff} . In general, the phase of the hypotrochoid that corresponds to the leading eigenvalue is a solution of $U_{\alpha-2}(\cos(\phi^*)) = -(\rho(\alpha - 1))^{-1}$, where $U_\alpha(x)$ are the Chebyshev polynomials of the second kind. For $\rho \geq \rho_f \equiv -(\alpha - 1)^{-2}$, and $\phi^* = 0$, while for $\rho < \rho_f$ the solution ϕ^* for the leading edge of the approximate eigenvalue support has a more complex form. Then g_{eff} is the real part of the support at ϕ^* . For $\alpha = 3$,

$$g_{\text{eff}} \equiv \begin{cases} g(1 + \rho) & \rho \geq \rho_f = -0.25 \\ -g(\rho + 1/(8\rho)) & \rho < \rho_f = -0.25. \end{cases} \quad (3)$$

When $g_{\text{eff}} \lesssim 1$ the fixed point $\mathbf{x} = \mathbf{0}$ is stable. This “quiescent” fixed point becomes unstable when the real part of the leading eigenvalue is greater than 1, so the onset of nontrivial dynamics occurs at $g_{\text{eff}} \approx 1$. In large networks with uncorrelated weights, high-dimensional chaotic activity emerges as soon as the quiescent fixed point becomes unstable [1].

In contrast to networks with uncorrelated weights, we find that high-order cyclic correlations ($\alpha \geq 3$) suppress the emergence of chaotic activity near the onset of nontrivial dynamics. Fig. 1 Shows results for networks with $\alpha = 3$ and $N = 1600$ neurons. Figs. 1(a)–(b) show representative network activity near this onset. When weights are uncorrelated, $\rho = 0$, chaotic activity emerges near the onset of instability of the origin, and persists when correlations are weak and positive, $\rho \approx 0.23$. However, solutions typically converge to a fixed point when correlations are strong ($\rho \approx 0.76$ in Fig. 1(b)). Similarly, chaotic activity persists when correlations are weak and negative, $\rho \approx -0.23$, but is replaced by high frequency oscillations when correlations are strong and negative, $\rho \approx -0.76$.

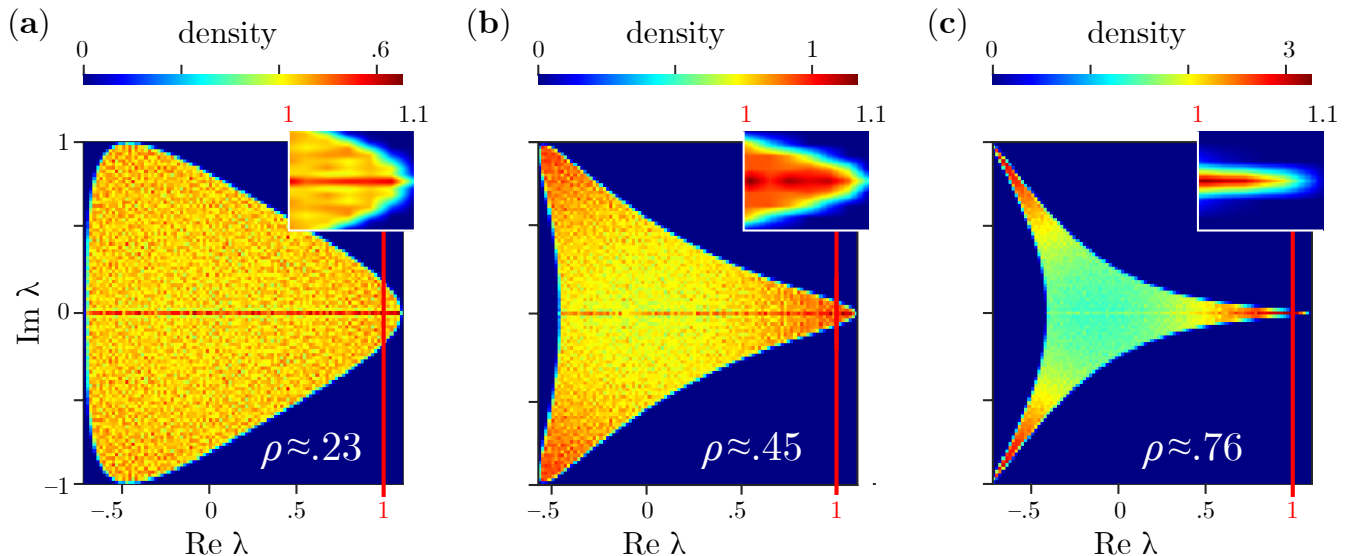


FIG. 2: Distribution of random connectivity matrix eigenvalues when $g_{\text{eff}} = 1.1$ for (a) $\rho \approx 0.23$, (b) $\rho \approx 0.45$, and (c) $\rho \approx 0.76$. Red lines at $\text{Re } \lambda = 1$ mark limit of stability for eigenvalues. Insets show expanded views of the distributions of the unstable eigenvalues at the tips that control the network dynamics.

Figure 1(c) shows the probability of observing chaotic, oscillatory, or fixed point dynamics as g_{eff} and ρ are varied with the intensity of the different colors representing the empirical probability of finding each state. To obtain these probabilities we smoothed the results from 300 simulations at each point of a parameter grid with spacings $\Delta g_{\text{eff}} \approx 0.29$ and $\Delta \rho \approx 0.08$, with each simulation using a different network realization (See section IB for details.) The fact that oscillations or fixed points are sometimes found near the onset of instability of the quiescent fixed point when $|\rho| < \rho_c$ is likely a finite size effect. The range of g_{eff} for which we find fixed points or oscillations after this onset decreases in width as $1/\sqrt{N}$ for $\rho = 0$ [1]. We find that this range also decreases with N for $|\rho| < \rho_c$. (See Fig. S3(a)-S3(b).)

In recurrent neural networks, the dimensionality of attractors is constrained by the network architecture [19]. A common measure of dimensionality is the participation ratio normalized by network size [19, 43, 44]. Fig. 1(d) shows that this normalized participation dimension peaks at $\rho \approx -0.3$ for different values of g_{eff} , and decreases considerably from this peak at larger or smaller values of weight correlations, ρ . Thus, even when solutions are chaotic, third order cyclic correlations strongly impact network dynamics.

What causes the observed stabilization of network dynamics? We hypothesize that it is due to the distribution of unstable eigenvalues, *i.e.* eigenvalues λ with $\text{Re } \lambda > 1$. The shape of the support of the eigenvalue spectrum, which is approximately given by the hypotrochoid curve, changes with ρ . Fig. 1(a) shows examples for $\alpha = 3$. In general, the support has α “vertices”. The spectral distributions at ρ and $-\rho$ are identical up to a rotation by

π/α . For $\rho > \rho_f$, one of the vertices is aligned with the real axis, while for $\rho < \rho_f$, the real axis is half way between two vertices. When $|\rho| < \rho_c$, the hypotrochoid is smooth at the vertices, but when $|\rho| \geq \rho_c$, the hypotrochoid has cusps. This change in the morphology results in a phase transition in the dynamics at the onset of instability of the quiescent fixed point.

Figure 2 shows how the nonuniform eigenvalue density within the support changes as a function of ρ for $\alpha = 3$ (100 realizations, $N = 6400$). Eigenvalues accumulate near the tips of the vertices as $|\rho|$ increases. For all ρ there is an excess of real eigenvalues. For networks with pairwise correlations ($\alpha = 2$), this excess density is known to decay as $\sim 1/\sqrt{N}$ [2]. For weak correlations, the eigenvalue distribution is nearly uniform, *e.g.*, at $\rho \approx 0.23$ as shown in Fig. 2(a). As ρ increases, the eigenvalues accumulate near the tips of the vertices, *e.g.*, at $\rho \approx 0.45$ as shown in Fig. 2(b). However, for $\rho > \rho_c = 0.5$, when the vertices are cusps, the eigenvalue density is maximal at a point in the middle of each cusp, away from the tips. Here, the eigenvalue density decays slowly towards the tips from the maxima, as can be seen for $\rho \approx 0.76$ in Fig. 2(c).

The leading eigenvalues in the spectrum control the stability of the dynamics. For $\rho = 0$, the spectrum is given by the circular law [1, 45], and the leading eigenvalues are at the leading edge of the circle. In the limit of large N , many eigenvalues become unstable simultaneously at the onset of instability of the quiescent fixed point where $g_{\text{eff}} \approx 1^+$, leading to chaos [1]. The same appears to be true for all $|\rho| < \rho_c$: many eigenvalues become unstable simultaneously and chaotic dynamics emerge with high probability. For $\rho \approx \rho_f$, where the

leading edge of the spectrum is flat (vertical), dynamics has maximal dimensionality (See Fig. 1(d)). At this value of ρ , the probability of observing chaos when the origin becomes unstable is also maximal.

For $\rho > \rho_f$, the vertex at the leading edge of the support is along the real axis. As ρ increases, the vertex becomes increasingly pointed, the eigenvalues accumulate around the real axis, the magnitudes of their imaginary parts decrease, and the fluctuations in the dynamics slow. (See insets of Figs. 2(a) and 2(b).) For $\rho < \rho_f$, the leading edge of the spectrum occurs at two symmetric vertices on either side of the real axis. Here, as ρ decreases, the eigenvalues accumulate near the two vertices. In both cases, for $|\rho| > \rho_c$, when there are cusps at the tips of the vertices, eigenvalues do not accumulate at the edge of the support. Instead, the eigenvalue density decays toward the tips of the cusps. Because of this, the number of unstable eigenvalues increases slowly with g_{eff} after the onset of instability of the quiescent fixed point, even in the limit of large N . (See inset of Fig. 2(c).) This slow increase corresponds with the high probability of observing fixed points or oscillations in the dynamics. Thus, at $\rho = \pm\rho_c$, where there is a morphological change at the leading edge of the eigenvalue support, we conjecture that there are critical points where phase transitions in the dynamics at onset occur. This conclusion is consistent with what is known about networks with pairwise correlations ($\alpha = 2$), where chaos occurs at onset for all $|\rho| < 1$, but fixed point behavior occurs at $\rho = \rho_c = 1$ [21, 46].

Although chaotic dynamics do not occur at the onset of instability of the origin for strong correlations where $|\rho| > \rho_c$, it does appear when g_{eff} is large, e.g., for $|\rho| \approx 0.75$ chaos is still observed with high probability when $g_{\text{eff}} \gtrsim 3$ in Fig. 1(c). The value of g_{eff} for which chaos is first observed decreases as $|\rho| \rightarrow \rho_c$, presumably to $\sim 1^+$ in the limit of large N . However, simulations are complicated in this region because the transient time increases with both g_{eff} and N , and it becomes difficult to distinguish between chaotic behavior, and fixed point or oscillatory dynamics with long transients.

Numerical investigations of networks with $\alpha = 4, 5$ and 6 confirm the existence of phase transitions in the dynamics at onset and critical points at $\rho = \pm\rho_c$ consistent with the above predictions. However, at values of $|\rho| \gg \rho_c$, deviations from the Hypotrochoid Law become increasingly large with α . For these networks, at such high values of $|\rho|$, our approximation for the gain at the onset of nontrivial dynamics, g_{eff} , becomes inaccurate.

The network dynamics within the region where chaos is observed are strongly influenced by high-order correlations. Fig. 3 shows the average attractor dimensionality and Lyapunov exponents λ_{LE} as a function of α , at fixed values of $|\rho| \approx 0.18$ and g_{eff} . The data are averages over 50 realizations of networks with $N = 1600$. (See Fig. S4 for the corresponding representative eigenvalue distributions.) Both quantities behave similarly for both positive and negative correlations. For the positive value

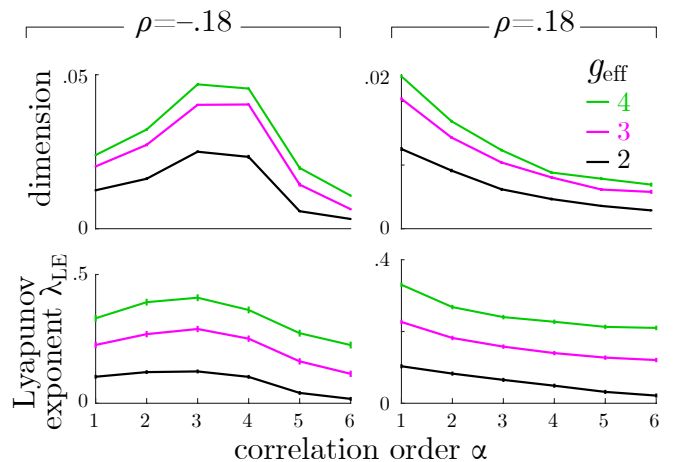


FIG. 3: Averaged normalized attractor dimension (top row) and corresponding Lyapunov exponents, λ_{LE} , (bottom row) as a function of α for different values of g_{eff} . ($\alpha = 1$ corresponds to uncorrelated networks.) The left and right columns show results with negative and positive correlations $\rho \approx \pm 0.18$, respectively.

of ρ , both quantities decrease monotonically with α . For the negative value of ρ , the quantities peak near $\alpha = 3$. For $\alpha \leq 3$, the correlation strength is greater than and approaching ρ_f , while for $\alpha > 3$, it is less than and diverging from ρ_f . These results are consistent with Fig. 1(d) that shows the largest dimensionality occurs at $\rho \approx \rho_f$, where the leading edge of the support is flat and many eigenvalues become unstable simultaneously at onset.

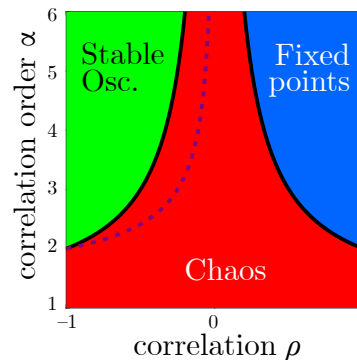


FIG. 4: Phase diagram of dynamics at the onset of the instability of the origin as a function of correlation strength ρ and correlation order α in the limit of $N \rightarrow \infty$. Solid lines correspond to $\pm\rho_c$, where the eigenvalue support of the synaptic connectivity matrix develops cusps. Dashed line corresponds to ρ_f , where the leading edge of the support is flat and the dimensionality of the dynamics is maximal.

Thus, we conjecture the phase diagram in Fig. 4 for the dynamics at the onset of instability of the quiescent fixed point as a function of ρ and α , where α is extended to a real variable. Lines of critical points (solid lines)

separate the chaotic phase (red) from the phases where fixed points (blue) and stable oscillations (green) occur. The dimensionality of the dynamics and the Lyapunov exponents are maximal along a line in the midst of the chaotic region (dashed line).

Real neural networks are known to have high-order cyclic synaptic correlations [11, 16, 24]. We have shown how these connectivity structures influence network dynamics by examining a minimal model of cortical networks designed to capture their essential effects. We show that networks with strong positive correlations have stable or weak chaotic dynamics, which are known to enhance computational performance [47–49]. Networks with strong negative correlations support robust oscillations, which are found across multiple brain regions (e.g., [50]). Further, the correlation among low-dimensional dynamics, weak chaos, and high-order structures suggests that low-dimensional activity regions in the brain may be highly structured. Furthermore, these findings may also provide insights into the macroscopic statistical properties of other disordered correlated systems, such as spin glasses [51–53], ecological networks [54, 55], and social networks [56].

Our work establishes a basis for exploring the computational benefits of high-order connectivity structures. Prior studies show that adding low-rank components to random matrices improves performance in discrimination tasks [20] and that specific phase-space patterns relate to learned tasks [57]. Our findings could lead to further improvements and link connectivity to phase-space dynamical motifs. This may illuminate cortical functionality and inspire advances in artificial learning models.

I. SUPPLEMENTARY MATERIALS

A. Matrix generation

To generate α -order cyclic correlations, we start with an $N \times N$ random matrix, where the entries are iid with $\sim \mathcal{N}(0, g^2/N)$. Next, we methodically change the sign of the corresponding entries such that the sum of all cycles of length α that end up in that specific entry would be positive with a probability P . This probability will determine the strength of the correlations ρ , see Fig. S1. We do the same for negative correlations but demand that the sum be negative. The step-by-step algorithm is shown in algorithm 1. Note that $w_{l,1:k}$ is a $1 \times k$ vector, and \odot is the element-wise product.

B. Numerical details of phase diagram

The probability of observing chaotic, oscillatory, or fixed point behavior was computed by averaging over 300 different network realizations with $N = 1600$. The condition for a fixed-point solution is that the derivative of the trajectories is less than 10^{-4} in the final 20% of

Algorithm 1: Generating high-order cyclic correlations

```

input :  $N \times N$  random matrix with
          $w_{ij} \sim \mathcal{N}(0, g^2/N)$ 
output:  $N \times N$  matrix with  $\text{Tr } W^\alpha/N = \rho > 0$ 
1 Initialize an  $N \times N$  random matrix, where the
  entries are iid with  $w_{ij} \sim \mathcal{N}(0, g^2/N)$ ;
2 for  $n = \alpha - 1 : N$  do
3    $\tilde{w} = (w_{n+1,1:n} w_{1:n,1:n}^{\alpha-2}) \odot w_{n+1,1:n}$ ;
4   for  $c = 1 : n$  do
5     if  $\tilde{w}_{c,n+1} < 0$  then
6        $w_{c,n+1} \rightarrow -w_{c,n+1}$  by a probability  $P$ ;
7     end
8   end
9 end

```

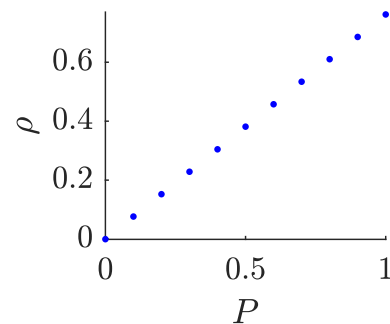


FIG. S1: Numerical value of ρ as a function of the probability P , averaged over 30 realizations.

the total runtime of the dynamics. Otherwise, we estimate the Lyapunov exponents with a cutoff of 0.01 to separate chaotic from oscillatory solutions. Colors were shaded based on their corresponding probabilities with red, green, and blue, for chaos, oscillations, and fixed points respectively.

ACKNOWLEDGMENTS

This research was supported in part by grants from NSF NeuroNex (DBI-1707400), NSF (DMS-2235451) and Simons Foundation (MPS-NITMB-00005320) to the NSF-Simons National Institute for Theory and Mathematics in Biology.

[1] H. Sompolinsky, A. Crisanti, and H.-J. Sommers, Physical review letters **61**, 259 (1988).

[2] H. J. Sommers, A. Crisanti, H. Sompolinsky, and Y. Stein, Physical review letters **60**, 1895 (1988).

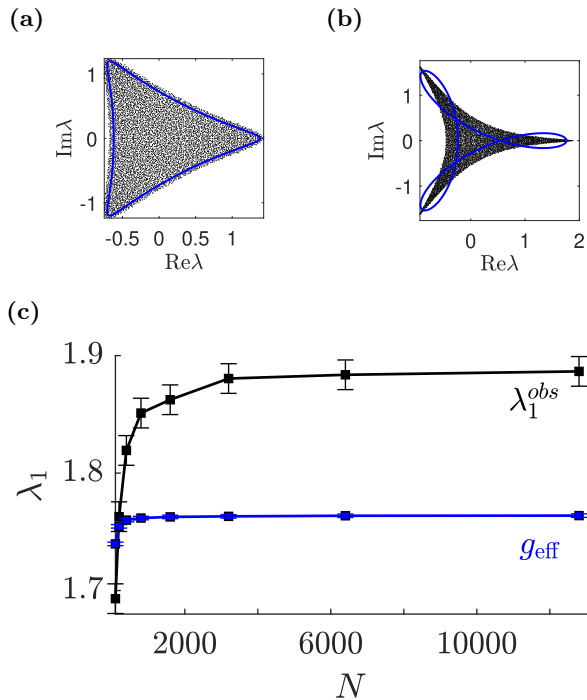


FIG. S2: (a) Eigenvalue distribution (black dots) shown for $\rho \approx 0.38$ with $N = 6400$. The blue curve depicts the equation of the support $z(\phi) = e^{i\phi} + \rho e^{-2i\phi}$. (b) The same as (a) but with $\rho \approx 0.76$. (c) The observed value of the real part of the rightmost eigenvalue, λ_1^{obs} (black) and g_{eff} (blue) as a function of N , with $g = 1$ and $\rho = 0.76$, averaged over 30 different realizations.

- [3] C. Van Vreeswijk and H. Sompolinsky, *Science* **274**, 1724 (1996).
- [4] K. Rajan and L. F. Abbott, *Physical review letters* **97**, 188104 (2006).
- [5] K. Rajan, L. Abbott, and H. Sompolinsky, *Physical review e* **82**, 011903 (2010).
- [6] J. Kadmon and H. Sompolinsky, *Physical Review X* **5**, 041030 (2015).
- [7] J. Aljadeff, M. Stern, and T. Sharpee, *Physical review letters* **114**, 088101 (2015).
- [8] A. Litwin-Kumar and B. Doiron, *Nature neuroscience* **15**, 1498 (2012).
- [9] J. G. White, E. Southgate, J. N. Thomson, S. Brenner, *et al.*, *Philos Trans R Soc Lond B Biol Sci* **314**, 1 (1986).
- [10] O. Sporns and R. Kötter, *PLoS biology* **2**, e369 (2004).
- [11] S. Song, P. J. Sjöström, M. Reigl, S. Nelson, and D. B. Chklovskii, *PLoS biology* **3**, e68 (2005).
- [12] E. Bullmore and O. Sporns, *Nature reviews neuroscience* **10**, 186 (2009).
- [13] H. Ko, S. B. Hofer, B. Pichler, K. A. Buchanan, P. J. Sjöström, and T. D. Mrsic-Flogel, *Nature* **473**, 87 (2011).
- [14] R. B. Levy and A. D. Reyes, *Journal of Neuroscience* **32**, 5609 (2012).
- [15] C. Duclos, D. Nadin, Y. Mahdid, V. Tarnal, P. Picton, G. Vanini, G. Golmirzaie, E. Janke, M. S. Avidan, M. B. Kelz, *et al.*, *Scientific reports* **11**, 3892 (2021).

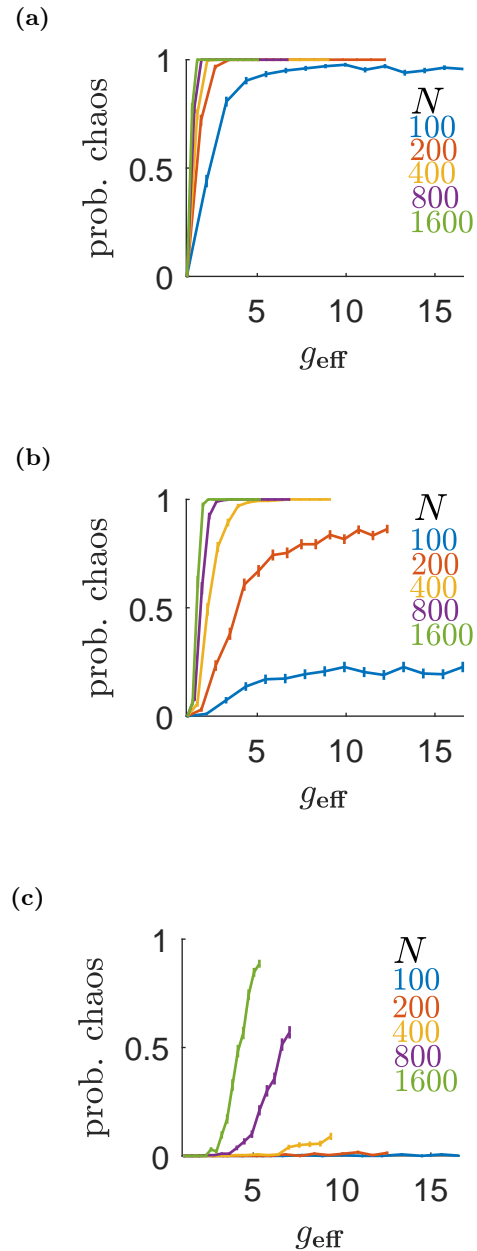


FIG. S3: Probability of observing chaos for different values of N with (a) $\rho \approx 0$, (b) $\rho \approx 0.23$, and (c) $\rho \approx 0.76$. Data was averaged over 300 different realizations of the connectivity matrix.

- [16] R. Yang, A. Vishwanathan, J. Wu, N. Kemnitz, D. Ih, N. Turner, K. Lee, I. Tartavull, W. M. Silversmith, C. S. Jordan, *et al.*, *Current Biology* **33**, 2340 (2023).
- [17] R. Rosenbaum, M. A. Smith, A. Kohn, J. E. Rubin, and B. Doiron, *Nature neuroscience* **20**, 107 (2017).
- [18] K. Berlemont and G. Mongillo, *bioRxiv*, 2022 (2022).
- [19] D. G. Clark, L. Abbott, and A. Litwin-Kumar, *Physical Review Letters* **131**, 118401 (2023).
- [20] F. Mastrogiuseppe and S. Ostojic, *Neuron* **99**, 609 (2018).
- [21] D. Martí, N. Brunel, and S. Ostojic, *Physical Review E* **97**, 062314 (2018).

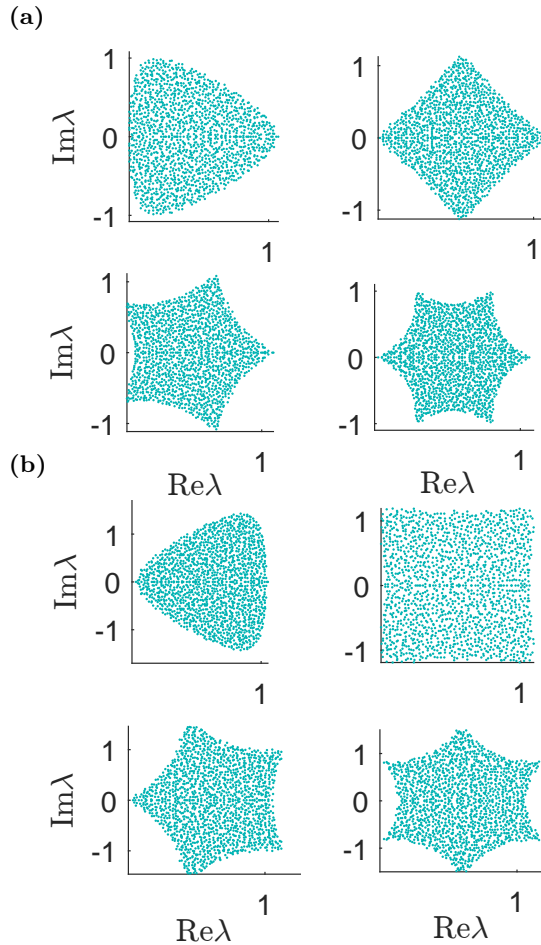


FIG. S4: Eigenvalue distributions for $\alpha = 3$ (top left), $\alpha = 4$ (top right), $\alpha = 5$ (bottom left), and $\alpha = 6$ (bottom right) with (a) $\rho \approx 0.18$, and (b) $\rho \approx -0.18$. Network size is $N = 1600$ and $g_{\text{eff}} \approx 1.1$.

- [22] R. Perin, T. K. Berger, and H. Markram, *Proceedings of the National Academy of Sciences* **108**, 5419 (2011).
- [23] O. Sporns, *Frontiers in computational neuroscience* **5**, 5 (2011).
- [24] Y. Wei, X. Liao, C. Yan, Y. He, and M. Xia, *Human brain mapping* **38**, 2734 (2017).
- [25] V. Pernice, B. Staude, S. Cardanobile, and S. Rotter, *PLoS computational biology* **7**, e1002059 (2011).
- [26] Y. Hu, J. Trousdale, K. Josić, and E. Shea-Brown, *Journal of Statistical Mechanics: Theory and Experiment* **2013**, P03012 (2013).
- [27] Y. Hu, J. Trousdale, K. Josić, and E. Shea-Brown, *Physical Review E* **89**, 032802 (2014).
- [28] L. L. Gollo and M. Breakspear, *Philosophical Transactions of the Royal Society B: Biological Sciences* **369**, 20130532 (2014).
- [29] L. L. Gollo, A. Zalesky, R. M. Hutchison, M. Van Den Heuvel, and M. Breakspear, *Philosophical Transactions of the Royal Society B: Biological Sciences* **370**, 20140165 (2015).
- [30] F. Battiston, E. Amico, A. Barrat, G. Bianconi, G. Ferraz de Arruda, B. Franceschiello, I. Iacopini, S. Kéfi, V. Latora, Y. Moreno, *et al.*, *Nature Physics* **17**, 1093 (2021).
- [31] S. S. Deshpande, G. A. Smith, and W. van Drongelen, *Scientific Reports* **13**, 238 (2023).
- [32] F. L. Metz, I. Neri, and D. Bollé, *Physical Review E* **84**, 055101 (2011).
- [33] D. Bollé, F. L. Metz, and I. Neri, *Spectral analysis, differential equations and mathematical physics: a festschrift in honor of Fritz Gesztesy's 60th birthday*, 35 (2013).
- [34] Y. Ahmadian, F. Fumarola, and K. D. Miller, *Physical Review E* **91**, 012820 (2015).
- [35] A. Kuczala and T. O. Sharpee, *Physical Review E* **94**, 050101 (2016).
- [36] P. V. Aceituno, T. Rogers, and H. Schomerus, *Physical Review E* **100**, 010302 (2019).
- [37] M. Helias and D. Dahmen, *Statistical field theory for neural networks*, Vol. 970 (Springer, 2020).
- [38] W. Zou and H. Huang, arXiv preprint arXiv:2305.08459 (2023).
- [39] S.-I. Amari, *IEEE Transactions on systems, man, and cybernetics*, 643 (1972).
- [40] J. Ginibre, *Journal of Mathematical Physics* **6**, 440 (1965).
- [41] V. L. Girko, *Theory of Probability & Its Applications* **29**, 694 (1985).
- [42] T. Tao, V. Vu, and M. Krishnapur, (2010).
- [43] S. Recanatesi, G. K. Ocker, M. A. Buice, and E. Shea-Brown, *PLoS computational biology* **15**, e1006446 (2019).
- [44] S. Recanatesi, S. Bradde, V. Balasubramanian, N. A. Steinmetz, and E. Shea-Brown, *Patterns* **3** (2022).
- [45] T. Tao and V. Vu, *Communications in Contemporary Mathematics* **10**, 261 (2008).
- [46] A. Crisanti and H. Sompolinsky, *Physical Review E* **98**, 062120 (2018).
- [47] N. Bertschinger, T. Natschläger, and R. Legenstein, *Advances in neural information processing systems* **17** (2004).
- [48] R. Laje and D. V. Buonomano, *Nature neuroscience* **16**, 925 (2013).
- [49] L. Kozachkov, M. Lundqvist, J.-J. Slotine, and E. K. Miller, *PLoS computational biology* **16**, e1007659 (2020).
- [50] K. Mizuseki and H. Miyawaki, *Neuroscience Research* **189**, 3 (2023).
- [51] D. Larson, H. G. Katzgraber, M. Moore, and A. Young, *Physical Review B—Condensed Matter and Materials Physics* **81**, 064415 (2010).
- [52] M. Bagherikalhor, B. Askari, and G. Jafari, arXiv preprint arXiv:2304.13692 (2023).
- [53] M. Mézard, *Indian Journal of Physics* **98**, 3757 (2024).
- [54] T. J. Case and E. A. Bender, *The American Naturalist* **118**, 920 (1981).
- [55] E. Bairey, E. D. Kelsic, and R. Kishony, *Nature communications* **7**, 12285 (2016).
- [56] F. Battiston, G. Cencetti, I. Iacopini, V. Latora, M. Lucas, A. Patania, J.-G. Young, and G. Petri, *Physics reports* **874**, 1 (2020).
- [57] L. N. Driscoll, K. Shenoy, and D. Sussillo, *Nature Neuroscience* **27**, 1349 (2024).